Perylenes as sensitizers in hybrid solar cells

Li, Chen; Liu, Zhihong; Schoneboom, Jan; Eickemeyer, Felix; Pschirer, Neil G.; Erk, Peter; Herrmann, Andreas; Mullen, Klaus; Schöneboom, Jan; Grätzel, Michael

Published in:
Journal of Materials Chemistry

DOI:
10.1039/b823498a

Publication date:
2009

Perylenes as sensitizers in hybrid solar cells: how molecular size influences performance†

Chen Li,[a] Zhihong Liu,[a] Jan Schöneboom,[b] Felix Eickemeyer,[b] Neil G. Pschirer,[b] Peter Erk,[b] Andreas Herrmann[c] and Klaus Müllen*[a]

Received 6th January 2009, Accepted 15th April 2009
First published as an Advance Article on the web 18th May 2009
DOI: 10.1039/b823498a

Dye-sensitized solar cells (DSCs), one kind of hybrid solar cells, are being intensively developed due to their high efficiency and low cost. One of the main factors to improve the efficiency is the minimization of the recombination of holes and electrons at the TiO_2/dye/electrolyte interface. To suppress the charge recombination, dye arrangement on the TiO_2 surface plays the pivotal role in DSCs. Herein we report three perylene sensitizers of various molecular sizes, which are derived from the introduction of different groups in the 1,6-positions of the perylene core. The same donor (di-*p*-*tert*-octylphenylamino) and acceptor (anhydride) moieties in these perylene sensitizers render them highly similar spectroscopic and electrochemical properties, which can be used to compare the effect of the dye-loading on the TiO_2 surface, namely, the photovoltaic performance as a function of the sensitizer size. These results will help in better understanding the complex relationship between the molecular size and the device performance.

Introduction

Dye-sensitized solar cells (DSCs) have evolved as a promising alternative to conventional silicon-based solar cells because of their high power conversion efficiency, short energy payback time and high semiconductor stability.[1,2] In principle, a DSC comprises a sensitizer dye coated onto a nanocrystalline metal oxide film (for example, TiO_2 or ZnO) and filled with hole-transport materials such as iodide/triiodide redox liquid electrolyte. In order to obtain high power conversion efficiency in DSCs, significant efforts are under way to optimize the charge transfer kinetics at the TiO_2/dye/electrolyte interface (Scheme 1).[3,4] Efficient operation of the DSCs depends on the minimization of the possible recombination pathways which occur at the interface. There are two primary interfacial recombination pathways: the electrons which inject into the conduction-band of TiO_2 may recombine either with oxidized dye molecules or with redox species in the electrolyte as illustrated in Scheme 1.[5]

Due to the rapid reduction of ionized dye molecules by iodine ions, which are present at high concentration, the contribution of this energy-loss channel to the recombination current can usually be ignored,[5] so that the recombination reaction occurs almost entirely at the TiO_2/electrolyte interface. Therefore, the back reaction can theoretically be blocked by surface modifications, such as introducing an insulating layer on the solvent-exposed parts of the TiO_2 film in order to obtain the passivation of the interface,[6,7] using core-shell structured particles instead of bare TiO_2,[8–10] or introducing co-adsorbents to form a more compact monolayer.[11,12] Another alternative is to achieve a highly covered nanoporous electrode through optimising the dye structures, which also retains the ease of device fabrication. It is known that the addition of aliphatic chains to the sensitizer dyes, including both ruthenium complexes[13] and organic metal-free dyes,[14] can result in a significant retardation of the recombination reaction between the redox electrolyte and the TiO_2 surface, thus giving rise to higher photovoltaic performance.

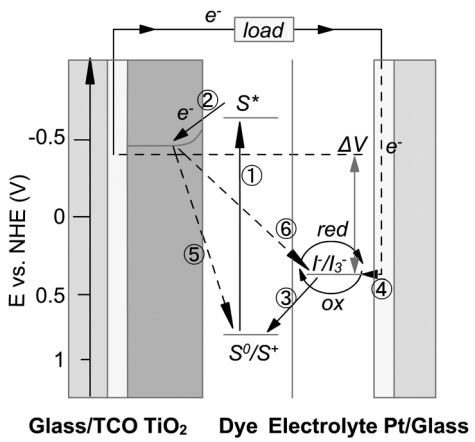

Scheme 1 Schematic representation of the operation mechanism of dye-sensitized solar cells showing photogeneration of the exited state of the sensitizers, electron injection into the conduction band of nanoporous TiO_2, regeneration of the dye ground state by electron transfer from the iodide/triiodide redox couple, regeneration of the redox couple by electron injection from the cathode, recombination at the TiO_2/dye interface, and recombination at the TiO_2/electrolyte interface.

In this paper, we vary the sizes of the sensitizer molecules of a very stable dye class and report the corresponding change in solar cell properties. Perylene dyes are well known as a key

[a]*Max Planck Institute for Polymer Research, 55128 Mainz, Germany*
[b]*BASF SE, Research Specialty Chemicals, D-67056 Ludwigshafen, Germany*
[c]*Department of Polymer Chemistry, Zernike Institute for Advanced Materials, University of Groningen, Nijenborgh 4, 9747 AG Groningen, Netherlands*

† This paper is part of a Journal of Materials Chemistry theme issue on solar cells. Guest editors: Michael Grätzel and René Janssen.

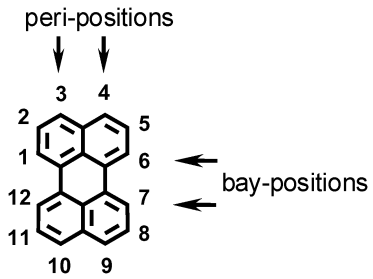

Fig. 1 Perylene structure.

chromophore among metal-free dyes.[15–36] Their solubility, absorption and emission behavior can be efficiently controlled by using a variety of synthetic procedures, which include the functionalization of *peri* or *bay* positions of the perylene core (Fig. 1).[37,38] Moreover, due to their outstanding photophysical and photochemical stability as well as their high fluorescence quantum yields, perylenes have been used as excellent materials for single molecule spectroscopy.[39] The same set of favorable properties also makes perylenes important active components for application in organic electronic devices.[40–56]

Recently, a successful approach was introduced by attaching a bulky nonplanar di-*p*-*tert*-octylphenylamino and an anhydride moiety to the perylene core, which not only suppresses the aggregation of dye molecules but also improves the stability of the organic sensitizer.[57,58] With two additional phenylthio groups in the 1,6-positons of the perylene unit, a new perylene sensitizer yields 87% incident monochromatic photon-to-current conversion efficiency (IPCE) and 6.8% power conversion efficiency under standard AM 1.5 solar conditions.[57] Here we demonstrate three perylene dyes with different molecular sizes (see Fig. 2), which are 9-di(*p*-*tert*-octylphenyl)amino-perylene-3,4-dicarboxy monoanhydride (ID28), 9-di(*p*-*tert*-octylphenyl)amino-1,6-diphenoxy-perylene-3,4-dicarboxy monoanhydride (ID96), and 9-di(*p*-*tert*-octylphenyl)amino-1,6-di(tetraphenyl)phenylphenoxy-perylene-3,4-dicarboxy monoanhydride (ID115). The only difference among these dyes comes from the substituents in the bay, which are hydrogen (ID28), phenoxy (ID96), and (tetraphenyl)phenyl-phenoxy (ID115). These groups serve as "molecular size controllers" leading to a different coverage of sensitizer dyes on the TiO_2 surface.

Results and discussion

Synthesis

These three perylene sensitizers are readily synthesized in high yields, which is illustrated in Scheme 2 and 3. The synthesis of ID28 was described in a previous article.[58] By selective bromination in the *bay* and *peri* region of *N*-(2,6-diisopropylphenyl)-perylene-3,4-dicarboximide with bromine in chloroform, the tribromo-substituted perylene derivative **1** can be synthesized.[59] After nucleophilic exchange of the bromines by phenolate, the desired compound **2** is obtained.[60,61] Compound **2** reacts further with *p*,*p*′-di-*tert*-octyldiphenylamine under Buchwald–Hartwig cross coupling conditions to provide the "push-pull" type molecule **4**. After saponification of **4**, perylene sensitizer ID96 is achieved (Scheme 2).

Compound ID115 is synthesized by applying the protocol used for the synthesis of dendronized perylene tetracarboxy diimides which has been reported by our group.[62,63] *Via* a Buchwald cross-coupling reaction and subsequent saponification of **6**, ID115 is obtained (Scheme 3).

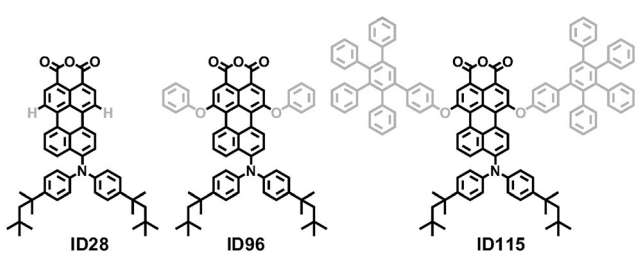

Fig. 2 Molecular structures of perylene sensitizer ID28, ID96 and ID115.

Photophysical and electrochemical properties

The absorption spectra of the dyes in solution and adsorbed on TiO_2 are shown in Fig. 3, and λ_{max} values are summarized in Table 1. In solution, ID96, ID115 as well as ID28 are blue compounds exhibiting charge-transfer and π–π^* transition bands in the range of 430–750 nm (Fig. 3). Different from ID28, ID96 and ID115 show an additional band at 350–430 nm due to the phenoxy groups in the 1,6-positions of the perylene core. However, ID96 and ID115 still retain the spectral signature of ID28 while improving the absorption coefficient. The absorption maxima of ID28, ID96 and ID115 occur at 606 (23 130 $M^{-1}cm^{-1}$), 605 (26 718 $M^{-1}cm^{-1}$) and 606 nm (24 996 $M^{-1}cm^{-1}$), respectively. The tiny difference of their absorption reveals that these three perylene dyes have similar S_1 transitions.

Due to the varying size of the different substituents in the 1,6-positions of the perylene core, different adsorption abilities of these dyes on TiO_2 films should arise. The adsorption of the dye on the TiO_2 surface is achieved by immersing the transparent TiO_2 film with 10 micron thickness on glass in a dye bath of dichloromethane solution (0.5 mmol L^{-1}) for 10 h, followed by rinsing with dichloromethane to remove unadsorbed dye and drying with argon to remove the solvent. The study of ID28 has disclosed that when the dye is absorbed onto TiO_2, a blue-shifted absorption can be detected which results from the ring opening of the anhydride groups.[58,64] The same blue shifts are observed upon treatment of the dyes with alkali, such as Na_2CO_3 in THF solution, forming the disodium salts of the dyes. Quantum mechanical calculations with the Turbomole program, using time-dependent density functional theory (TD-DFT) calculations at the B3-LYP/def-SV(P) level, show a blue-shifted absorption of the disodium salts as a result of reduced effective conjugation length and the push-pull effect (Table 1). With the same donor–acceptor functionalized perylene core, ID96 and ID115 also demonstrate a blue-shifted absorption on the TiO_2 surface (Fig. 3). Going from ID28 → ID96 → ID115, a decrease of the absorption intensity was observed. This is consistent with the increasing molecular weight of 713.97, 898.17 and 1056.96 g mol^{-1} respectively, and also corresponds to the different groups in the 1,6-positions of the perylene core, that is hydrogen, phenoxy and (tetraphenyl)phenylphenoxy, respectively. Therefore, the absorption wavelengths of these perylene dyes on the TiO_2 film is mainly attributed to the donor and acceptor substituents

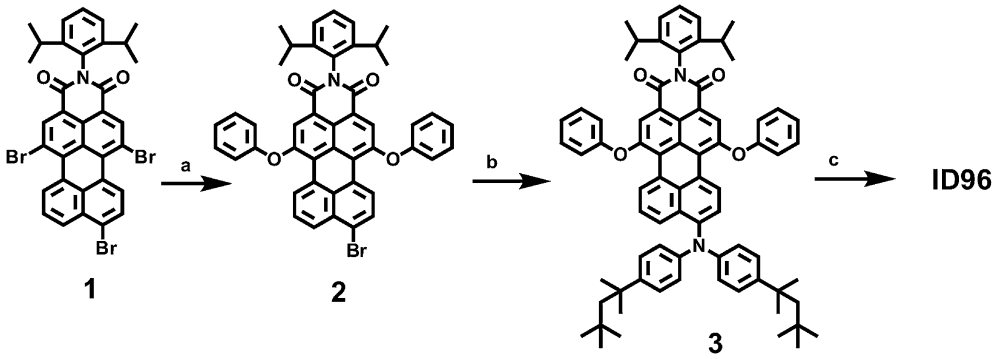

Scheme 2 Synthesis of ID96: (a) K_2CO_3, NMP, phenol, 65%; (b) *p*,*p*′-di-*tert*-octyldiphenylamine, $Pd_2(dba)_3$, *t*-BuONa, P(*t*-Bu)$_3$, toluene, 80 °C, overnight, 85%; (c) KOH, isopropanol, reflux, overnight, 80%.

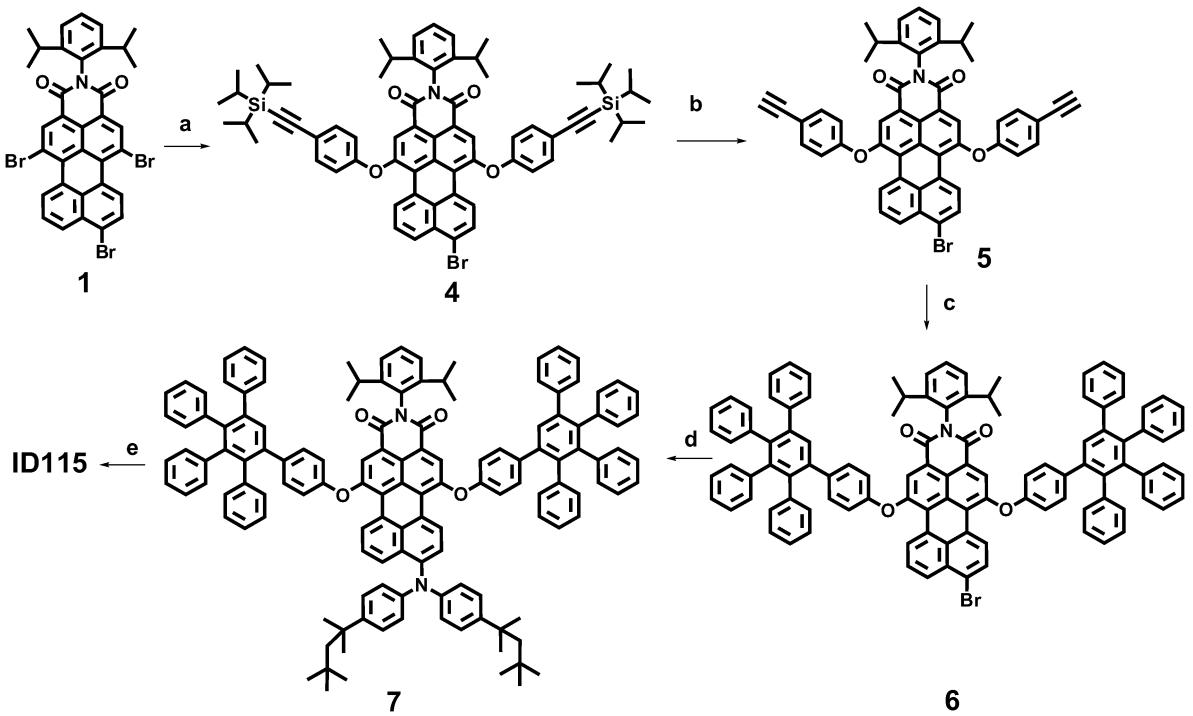

Scheme 3 Synthesis of ID115. (a) 4-((triisopropylsilyl)ethynyl)phenol, K_2CO_3, NMP, 80 °C, 5 h, 58%; (b) *n*-tetrabutylammonium fluoride, THF, r.t. 0.5 h, 70%; (c) tetraphenylcyclopentadienone, *m*-xylene, reflux, overnight, 75%; (d) $Pd_2(dba)_3$, *t*-BuONa, P(t-Bu)$_3$, *p*,*p*′-di-*tert*-octyldiphenylamine, toluene, 80 °C, 12 h, 82%; (e) KOH, isopropanol, reflux, overnight, 60%.

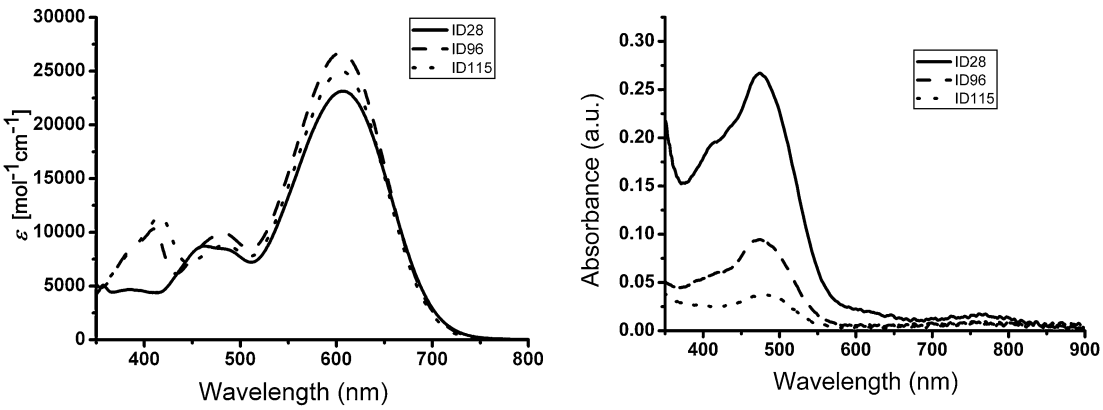

Fig. 3 Absorption spectra of the perylenes in dichloromethane solution (left) and adsorbed on TiO_2 film (right). The adsorption of the dye on the TiO_2 surface is achieved by immersing the transparent TiO_2 film with 10 micron thickness on glass in a dye bath of dichloromethane solution (0.5 mmol L^{-1}) for 10 h, followed by rinsing with dichloromethane to remove unadsorbed dye and drying with argon to remove the solvent.

Table 1 Electrochemical properties

	Exp (eV)				Calc. (eV)[c]					
					Ring Close			Ring Open		
Dye	HOMO[a]	LUMO[b]	In DCM λ_{max}/nm	On TiO_2 λ_{max}/nm	HOMO	LUMO	λ_{max}/nm	HOMO	LUMO	λ_{max}/nm
ID28	−5.25	−3.20	606	473	−6.42	−4.45	631	−5.74	−3.50	553
ID96	−5.19	−3.14	605	473	−6.09	−4.18	649	−5.58	−3.34	553
ID115	−5.22	−3.17	606	481	−5.91	−3.98	642	−5.45	−3.18	546

[a] Obtained by cyclic voltammetry in dichloromethane. [b] Estimated LUMO energies: obtained from the ground-state oxidation potential by adding the $E_{optical\ excitation\ energy}$, which was determined by the absorption spectrum in dichloromethane. [c] Calculated TD-DFT results.

in the *peri*-positions of the perylene core, while the substituents in the 1,6-positions of the perylene core effect the absorption coefficient as well as the width of the absorption band on TiO_2 film. The dye with smaller *bay*-substituents displays a broader absorption band on TiO_2 hinting towards possible aggregation. The relationship between aggregation and device performance will be the focus of a future investigation.

Redox properties

In DSCs, the energy-level matching is a crucial principle for designing new sensitizers. Examination of the optical properties of these dyes reveals that the side substituents in the 1,6-positions of the perylene core do not significantly influence the respective absorption properties. To gain further insight into the electronic characteristics of these three dyes, cyclic voltammetry (CV) is performed in dichloromethane solution (Fig. 4 and Table 1). The CV spectrum of ID28 shows one reversible oxidation wave at 0.6 V *vs.* Fc/Fc^+ (Fc: ferrocene) and one quasi-reversible reduction wave at 1.25 V. In the case of ID96 and ID115, the two reversible oxidation peaks detected at 0.6 and 1.0 V are due to the diphenylamino and phenoxy moieties. However, the additional oxidation peaks of ID96 and ID115 will not affect their ground state energy, since only the first oxidation peak is related to the HOMO level of the dyes. The same oxidation and reduction onsets, which are 0.4 and −1.6 V *vs.* Fc/Fc^+, respectively, indicate that the HOMO and LUMO energy levels of ID28, ID96 and ID115 are identical (Table 1).

Considering that all these perylene dyes show a blue-shifted absorption when adsorbed onto TiO_2, the shift of the absorption wavelength upon ring opening may be taken as a measurement of the redox potential change of the dyes on TiO_2. Comparing the DFT calculation results with the CV result in the ring closed form, the calculations apparently overestimate the shift to negative potentials in these dyes, especially for ID96 and ID115 (Table 1). The driving force for the injection of charge from the dye into the conduction band of TiO_2 or from the electrolyte to the dye is estimated to be very similar for ID96 and ID115 because (i) the identical anchoring groups ensure that the dyes have identical orientation on the TiO_2 surface (here we assume that the effect of the phenoxy group on the orientation of each dye on TiO_2 surface is negligible; the phenoxy groups only cause different stacking of dye molecules on the TiO_2 surface) and (ii) their same donor and acceptor groups render them similar LUMO/HOMO energy levels. It can be concluded that the different substituents in the 1,6-positions of the perylene core do not severely influence the driving force of the charge injection at the TiO_2/dye/electrolyte interface.

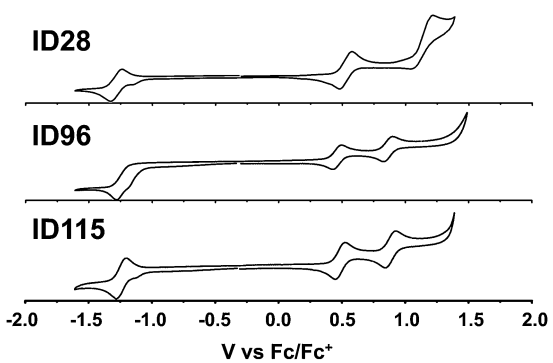

Fig. 4 Cyclic voltammograms of ID28, ID96 and ID115.

Molecular size measurements and calculation

Due to their similar photophysical and electrochemical properties it becomes important to investigate the size influence of the substituents in the 1,6-positions of the perylene core. To specify the effect, the area covered by the adsorbed dye on the TiO_2 surface is first determined by the concentration of the dye on the TiO_2 film and the intrinsic area of the TiO_2 film. The amount of dye is calculated from the UV-Vis spectrum of the remaining dye in the dye bath and also corrected for the amount of detached dye upon subsequent rinsing. The internal area of the TiO_2 electrodes is obtained from BET[65] measurements.

Table 2 gives the result of the dye-loading measurements and the calculation results of the dye-occupied area size on the TiO_2 surface. The experimental result (Table 2) gives an average molecular size which increases in the sequence ID28 → ID96 → ID115. The theoretical results (Fig. 5 and Table 2) are obtained by neglecting the influence of the molecular orientation on the TiO_2 surface and specific interactions between dye molecules. Both the experimental data and the computer estimates follow the trend of increasing molecular weight and decreasing absorption intensity of the dyes on the TiO_2 surface. The identical conclusion from the experimental and calculated results is that the substituents cause these dyes to have different loading behavior on the TiO_2 surface. Due to the size of the bay substituents, the loading concentration of the dyes on the TiO_2 electrodes is different, which alone will give rise to a different photovoltaic performance in the solar cells.

Table 2 Dye loading measurement. The amount of dye is calculated from the UV-Vis spectrum of the remaining dye in the dye bath and also corrected for the amount of detached dye upon subsequent rinsing. The internal area of the TiO_2 electrodes is obtained from BET[65] measurements

Dye	M.W.	Dye/area ($1/nm^2$)	Area/dye (nm^2)	Area/dye (calc.) (nm^2)
ID28	71 397	1.08	0.93	1.27
ID96	89 817	0.75	1.32	1.49
ID115	165 910	0.60	1.66	2.40

Photovoltaic performances

Dye sensitized solar cells are fabricated under identical conditions. The photocurrent action spectra (Fig. 6) and *I–V* curves (Fig. 7) of the devices containing these dyes are obtained using an electrolyte comprising tetrabutyl-ammonium iodide (0.25 M), LiI (0.5 M), I_2 (0.05 M) and 4-tertbutyl pyridine (0.5 M) in acetonitrile. The incident-photon-to-current conversion efficiencies (IPCE) maxima of ID28, ID96 and ID115 are 64%, 56% and 51%, respectively. The decrease of IPCE in the series ID28 → ID96 → ID115 can be explained by diminished electron injection resulting from the significantly lower dye concentration on the TiO_2 film in the case of larger molecular size. However, it can be noticed that there is a non-proportional decrease in IPCE of these three compounds devices when compared to their absorption spectra on TiO_2. To further investigate, we normalized the IPCE value according to molecular size (normalized IPCE = IPCE/(dye/area), Fig. 6). Interestingly, ID115 shows the highest normalized IPCE maximum up to 85%nm^2 while ID28 gives the lowest value. Additionally, the device of ID28 exhibits the broadest IPCE spectrum, possibly due to aggregation of ID28. Therefore, the molar amount of dye in the devices correlates with the observed photocurrent, where the dye content corresponds to the dye-loading performance and calculated dye occupation area; however, the normalized IPCE spectra illustrate that not all of the smaller dye molecules will contribute to photocurrent (Table 2).

Furthermore, the dyes with phenoxy groups (ID96 and ID115) show higher V_{oc} values (533 and 506 mV under 10% sun irradiation, 636 and 633 mV under 1 sun irradiation) when compared to ID28 (499 mV under 10% sun irradiation and 578 mV under 1 sun irradiation). Previous studies have shown that the perylene sensitizers with phenoxy groups in the bay positions can lead to a smaller dark current compared with that of ID28.[58] The reduction in dark current at a certain potential can originate from (i) higher conduction band (CB) in the TiO_2 and thus less electron population in the CB or (ii) improved charge recombination blocking in the TiO_2/dye/electrolyte interface.[13,14,66] Additionally, it is known that the key V_{oc}-limiting factor in DSCs is charge recombination of electrons on the TiO_2 with redox electrolyte (step 6, Scheme 1).[11–13] With the total consideration of

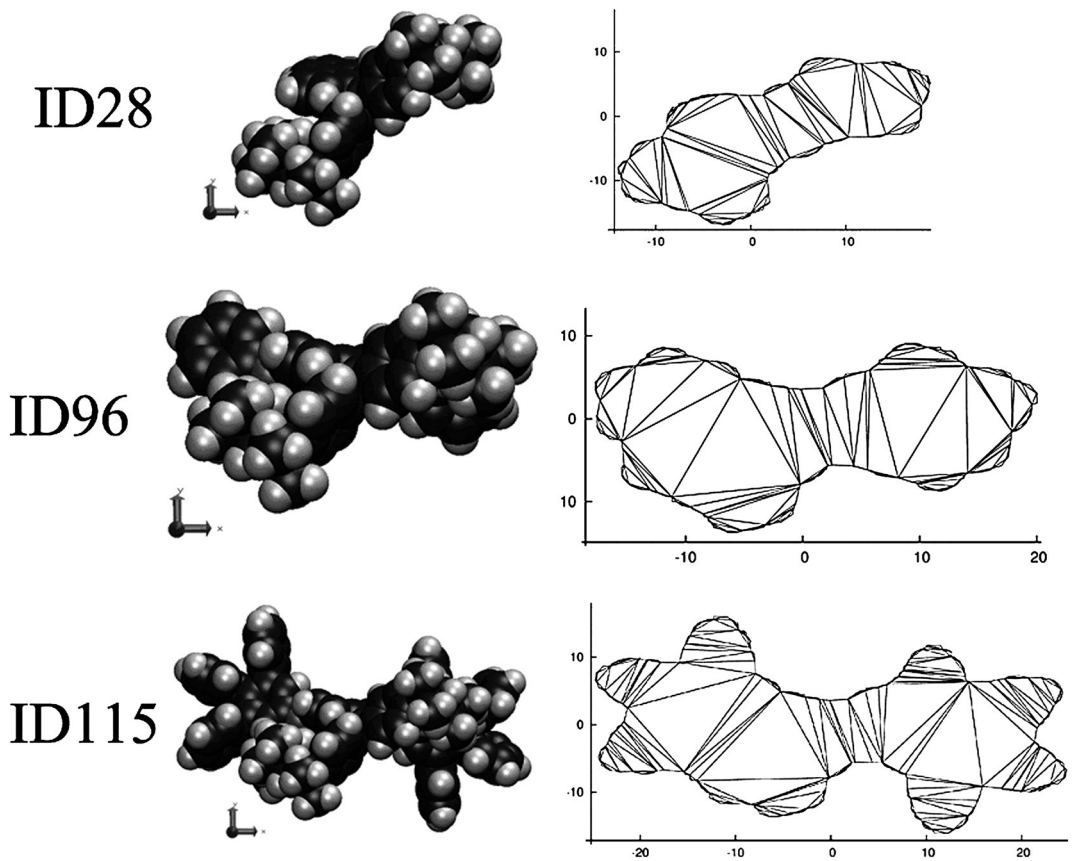

Fig. 5 Computational assessment of the minimum surface area per dye molecule. The three-dimensional van-der-Waals surface of the dyes (left panel) is projected along the long molecular axis, assuming a perfectly perpendicular arrangement of dyes on the surface. The resulting surface area (right panel) is evaluated by triangulation.

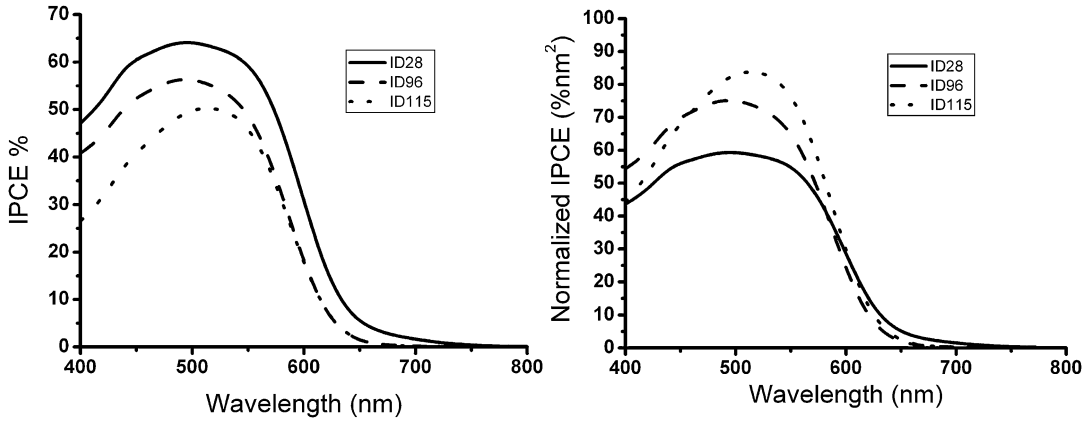

Fig. 6 IPCE (left) and normalized IPCE (right) spectra of ID28, ID96 and ID115. Electrolyte: tetrabutyl-ammonium iodide (0.25 M), LiI (0.5 M), I_2 (0.05 M) and 4-*tert*butyl pyridine (0.5 M) in acetonitrile.

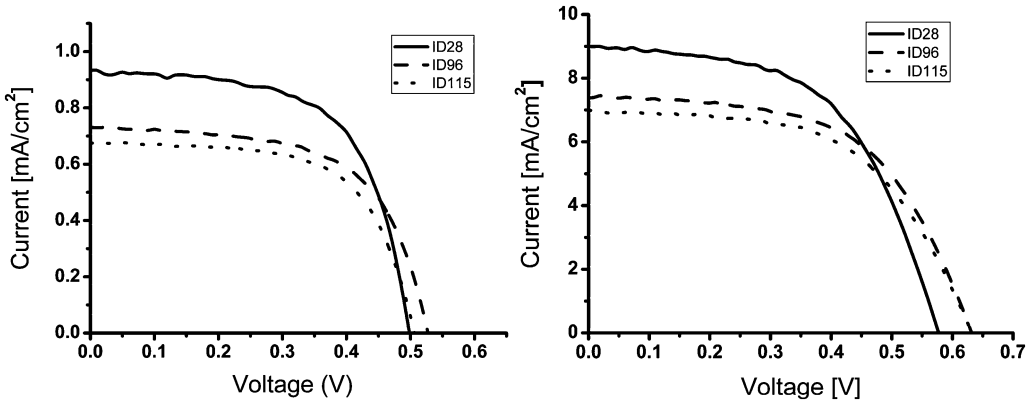

Fig. 7 Photocurrent density and voltage characteristics of DSCs prepared with perylene sensitizers: Irradiance: 10 mW cm^{-2} (left); 100 mW cm^{-2} (simulating AM 1.5) (right). Illuminated area: 0.50 cm^2. Film thickness: 10 μm. Electrolyte: tetrabutyl-ammonium iodide (0.25 M), LiI (0.5 M), I_2 (0.05 M) and 4-*tert*butyl pyridine (0.5 M) in acetonitrile.

the I_{sc}/V_{oc} values, absorption and molecular size, we infer that these phenoxy groups act in two ways: (i) generally increasing the molecular size and decreasing the concentration of the dye molecule on the TiO_2 surface, thus yielding a lower photocurrent response, and (ii) shielding the TiO_2 surface as barrier layer between TiO_2 and electrolyte interface. This suppresses the undesired recombination of electrons from the conduction band of TiO_2 with the redox electrolyte and thus improves the open-circuit voltage.

By comparing the photovoltaic performance of these perylene dyes at high and low intensities (Fig. 7 and Table 3), 0.1 sun and 1 sun, it is found that on one hand, the I_{sc} values are linearly proportional to the light intensity for each dye; on the other hand, the V_{oc}-changing values between 1 sun and 0.1 sun for ID28, ID96 and ID115 are 79, 103, 127 mV, respectively, which is related to the increasing size of the dye molecules. The trend in V_{oc} is also consistent with the improvement of the power conversion efficiency, which is 0%, 13% and 32% for ID28, ID96 and ID115, respectively. Combining all the photovoltaic results of these three perylene sensitizers, we found that (i) the IPCE/I_{sc} values do not correlate to the corresponding absorption properties of these dyes on TiO_2 surface. With the sensitizer molecular size increasing, the higher normalized IPCE values prove that a higher percentage of dyes are contributing to the photocurrent; (ii) all the devices based on these three dyes have a proportionally increased I_{sc} value under 10% sun compared to that under 1 sun irradiation, which proves that there is no charge injection problem in these cells; (iii) the improved V_{oc} of ID96 and ID115 could indicate less dark current in those cells. This would also explain the large increase of V_{oc} within the dye sensing at 1 sun, since recombination is strongly increased compared to that at 10% sun by electron density in TiO_2. It could be a result of a more uniform ordering or the possible prevention of aggregation *via* the *bay* substitutions. Currently investigations to understand this behavior, such as electron lifetime measurements are underway.

Conclusions

Here, three push-pull type perylene sensitizers, ID28, ID96 and ID115, with similar spectroscopic and electrochemical properties have been synthesized and used in dye-sensitized solar cells. The molecular size is controlled by the substituents in the *bay*-positions of the perylene core. The effect of sensitizer size on the performance of the solar cells has been studied. We have used UV-Vis absorption experiments to determine the average dye coverage on the TiO_2 surface and computer simulations to obtain

Table 3 Performance of DSCs using PMAs[a]

	Device performance under 0.1 Sun				Device performance under 1 Sun			
Dye	I_{sc}/mA cm^{-2}	V_{oc}/mV	FF (%)	η (%)	I_{sc}/mA cm^{-2}	V_{oc}/mV	FF (%)	η (%)
ID28	0.93	499	62	2.9	8.99	578	55	2.9
ID96	0.74	533	55	2.4	7.52	636	57	2.7
ID115	0.58	506	64	1.9	6.99	633	56	2.5

[a] Thickness of the TiO_2 film: 10μm. Irradiation area: 0.5 cm^2. Electrolyte: tetrabutyl-ammonium iodide (0.25 M), LiI (0.5 M), I_2 (0.05 M) and 4-*tert*butyl pyridine (0.5 M) in acetonitrile.

the molecular size. Without phenoxy groups, ID28 shows a much higher absorption coefficient and broader absorption band on TiO_2 film than that of the other two dyes, which is possibly due to the different aggregation and arrangement of ID28 on TiO_2 surface. This is under current investigation.

The device performance was tested under 0.1 sun or 1 sun irradiation in order to obtain more information on the molecular size effect. It was found that sensitizers with a smaller size show a better performance at low sun intensities. At higher light intensities, however, the efficiencies of the larger dyes (ID115) approached those of the smaller dyes (ID28) despite much less adsorption on TiO_2, suggesting the importance of the dye morphology on device performance, specifically regarding aggregation and recombination. In summary, these results shed light on the relationship between sensitizer geometry and device performance and provide an additional tool to improve the efficiencies of dye-sensitized solar cells.

Experimental

Measurement and characterization

^{1}H and ^{13}C NMR spectra were recorded on a Bruker AMX 300 NMR (300 and 75 MHz, respectively) with dichloromethane-d_2 as solvent and tetramethylsilane as internal standard. Chemical shifts were reported in parts per million. FD mass spectra were performed with a VG-Instruments ZAB 2-SE-FDP. Infrared spectra were recorded on a Nicolet FT-IR 320 spectrophotometer as KBr pellets. The elemental analyses were carried out by the Microanalytical Laboratory of Johannes Gutenberg University. The UV-Vis-NIR absorption measurements were performed on a Perkin-Elmer Lambda 15 spectrophotometer. The absorption spectra on the TiO_2 film were achieved by immersing the transparent TiO_2 film (TiO_2 paste used in all the experiments was obtained from Solaronix, Ti-Nanoxide HT/SP) with 10 micron thickness on glass in a dye solution in dichloromethane, followed by rinsing in dichloromethane to remove unadsorbed dye and by removing dichloromethane in a stream of argon. Cyclic voltammetry and differential pulse voltammetry were performed on an EG&G Princeton Applied Research potentiostat, model 273, in a solution of Bu_4NPF_6 (0.1 M) in dry dichloromethane with a scan rate of 50 mV s^{-1} at room temperature under argon. The working electrode consisted of an inlaid platinum disk (1.5 mm diameter) that was polished on a felt pad with 0.05 μm alumina and sonicated in milli-Q water for 5 min before each experiment. A platinum wire was used as the counter electrode and an Ag wire was used as the reference electrode internally calibrated with ferrocene/ferrocenium (Fc/Fc^+) in the measurement. From the potential of the oxidation onset, the HOMOs and LUMOs of the dyes can be estimated according to the eqn (1) and (2) ($E_{\text{optical excitation energy}}$ was determined by the absorption spectrum).

$$E_{\text{HOMO}} = -(E^{\text{ox}} + 4.8)\ \text{eV} \quad (1)$$

$$E_{\text{LUMO}} = E_{\text{HOMO}} + E_{\text{optical excitation energy}} \quad (2)$$

Quantum chemical calculations

Density functional theory (DFT) calculations were performed with the Turbomole program suite version 5.7.[67] Geometry optimizations were carried out with the BP86 functional[68] making use of the RI approximation.[69] The ionization potential (IP) was derived from a single point energy (BP86) of the positively charged radical cation at the relaxed geometry of the neutral dye molecule. Vertical optical excitation energies were obtained from time-dependent DFT (TDDFT) calculations[70,71] at the B3LYP level.[72] The def-SV(P) basis set was applied in all calculations.[73] The HOMO energy was calculated by using BP86/def-SV(P) (eqn (3)). The LUMO energy was estimated according to the eqn (2).

$$E_{\text{HOMO}} = E^{(\text{cation})}_{(\text{single point energy})} - E^{(\text{neutral})}_{(\text{optimized})} \quad (3)$$

Dye loading measurements and calculation of molecular size

The dye coverage loading on the TiO_2 surface was monitored by the absorption spectra. The TiO_2 film (25×13 mm^2) was coated on a conducting glass (Nippon Sheet glass, 10 Ω/square, 25×15 mm^2) and was immersed in the dye solution (0.5 mM) in dichloromethane for ten hours. The amount (n) of dye loaded on the nanoporous TiO_2 particle surface can be determined by the UV-vis spectrum of the remaining dye in the dye bath with correction for the detached dye upon subsequent rinsing. The internal area (t) of the TiO_2 electrodes was determined by BET measurements.[65] The average coverage of the dye was estimated according to eqn (3) (where A is the average coverage area of one molecule, M is the weight of the porous TiO_2 on the glass substrate, BET is the BET surface area of the porous TiO_2 nanocrystal, and N is the amount of the dye which was coated on the TiO_2).

$$A = (M \times \text{BET})/N \quad (3)$$

The theoretical estimates for the area occupied per dye molecule were obtained in the following way (Fig. 5): a conformational analysis of the flexible side-chains of the dye was performed with Macromodel torsional/low-mode sampling (Schrödinger Inc.). The lowest energy conformer was then oriented such that the perylene-monoanhydride moiety lies within the *xz* plane and the long molecular axis is along the *z*-direction. We constructed the van-der-Waals surface of the molecule (with the Turbomole program) as a set of points in Cartesian space. The projection of that volume in the *xy* plane then represents the surface area under one molecule, oriented perfectly perpendicular to the surface plane. We determined the concave envelope of the points in the *xy* plane with a probe radius of 2.0 Bohr. The size of the resulting area was then calculated by triangulation. This approach neglects specific surface structure characteristics, like Ti-vacancies or OH groups on the TiO_2 surface. It thus should give a lower limit of the true surface area per dye molecule.

Dye-sensitized solar cells

Nanostructured TiO_2 films (10 micron thick) on F-doped tin oxide coated glass (Nippon Sheet Glass Co., Ltd) were prepared by doctor blading a colloidal solution (20 nm sized anatase particles). The resulting layers were sintered at 450 °C for 30 min. Dye solutions were prepared in dichloromethane (500 mM) and titania electrodes were prepared by immersion in the dye solution for 12 h. The counter electrodes were made by spin-coating a 5 mM of H_2PtCl_6 isopropanol solution on a conducting glass and heating for 15 min at 380 °C, forming a light gray surface of nanoparticulate platinum on the conducting glass. The cells were sealed with a frame of Surlyn SX1170, 25 μm, by heating the clamped device at 120 °C for 7 min. The spectral response was measured with a xenon arc lamp (LOT LSB510) and a monochromator (ACTON SpectraPro-2150i). The overall photon-to-energy conversion efficiencies (η) were measured under Air Mass 1.5 (AM1.5) conditions using a 300 W xenon arc lamp (LOT LSB 530), calibrated with a reference Si-solar cell. The monochromatic incident photon-to-current conversion efficiency (IPCE) for solar cells is the ratio between the incoming photons at each wavelength and the photon generated electrons reaching the back contact in the device and is defined as

$$\mathrm{IPCE}(\lambda)[\%] = \frac{hc}{\lambda e}[\mathrm{eV}] \times \frac{J_{\mathrm{ph}}\left[\mathrm{mAcm}^{-2}\right]}{\Phi\left[\mathrm{mWcm}^{-2}\right]} \times 100$$

where h is Planck's constant, c the speed of light in vacuum, λ the wavelength, e the elementary charge, J_{ph} the short-circuit photocurrent density for monochromatic irradiation, and Φ the intensity of the incoming monochromatic light.

The current–voltage (*I–V*) curves were obtained under AM1.5 simulated solar irradiance (0.1 sun or 1 sun intensity).

Synthesis of sensitizers

The synthesis of *N*-(2,6-di*iso*propylphenyl)-1,6,9-tribromoperylene-3,4-dicarboximide (**1**) was performed as described before.[59] *p*,*p*′-Di-*tert*-octyldiphenylamine was purchased from MP Biomedicals Inc. All the other starting materials and catalysts were purchased from Aldrich, Acros, or ABCR, and used as received.

***N*-(2,6-Di*iso*propylphenyl)-1,6-diphenoxy-9-bromo-perylene-3,4-dicarboximide (2).** *N*-(2,6-di*iso*propylphenyl)-1,6,9-tribromoperylene-3,4-dicarboximide (3 g, 4.2 mmol), phenol (770 mg, 8.0 mmol) and potassium carbonate (1.1 g, 8.0 mmol) were stirred in NMP (300 mL) at 80 °C for 3 h. After cooling down to room temperature, the reaction mixture was poured into a mixture of water and hydrochloric acid (4 : 1). The resulting precipitate was washed with water and dried. The desired product was purified by column chromatography on silica gel using toluene as eluent to give a red solid (2 g, 65%).

^{1}H-NMR (250 MHz, CD_2Cl_2, 300 K): $\delta = 9.35$ (d, $J = 5$ Hz, 1H), 9.12 (d, $J = 8$ Hz, 1H), 8.26 (m, 3H), 7.84 (d, $J = 8$ Hz, 1H), 7.65 (m, 1H), 7.51–7.14 (m, 13H), 2.74 (m, 2H), 1.14 (d, $J = 7$ Hz, 12H) ppm; ^{13}C-NMR (75 MHz, CD_2Cl_2, 300 K) δ [ppm]: 163.5, 156.2, 156.1, 153.7, 153.6, 146.4, 132.2, 131.8, 131.4, 131.3, 131.0, 130.7, 129.7, 129.1, 128.2, 128.1, 127.7, 127.4, 127.2, 125.7, 125.1, 124.7, 124.6, 124.4, 123.8, 122.4, 122.3, 119.0, 29.4, 24.1. IR Spectrum (KBr): $\nu_{\max} = 2958$, 2866, 1705, 1668, 1589, 1485, 1414, 1331, 1271, 1201, 1070, 968, 876, 804, 752 cm^{-1}. UV-Vis (CH_2Cl_2): $\lambda_{\max}$ (ε/M^{-1} cm^{-1}): 512 (45 879). FD Mass Spectrum (8 kV): $m/z = 746.2$ (100%) [M$^+$] (calc. 744.69). Elemental analysis ($C_{46}H_{34}BrNO_4$): calculated: (%) C 74.19, H 4.60, N 1.88, found: (%) C 73.88, H 4.56, N 1.81.

***N*-(2,6-Di*iso*propylphenyl)-9-di(p-*tert*-octylphenyl)amino-1,6-diphenoxy-perylene-3,4-dicarboximide (3).** A mixture of **2** (500 mg, 0.67 mmol), *p*,*p*′-di-*tert*-octyldiphenylamine (395 mg, 1.0 mmol), tris-(dibenzylideneacetone)dipalladium(0) (50 mg, 0.05 mmol), tri-*tert*-butyl-phosphine (20 mg, 0.10 mmol), sodium-*tert*-butoxide (100 mg, 1 mmol) and dry toluene (100 mL) was stirred at 80 °C in an argon atmosphere overnight. The solvent was removed under evaporation. The crude product was purified by column chromatography using toluene as eluent on silica to give a blue solid (600 mg, 85%).

^{1}H-NMR (250 MHz, CD_2Cl_2, 300 K): $\delta = 9.31$ (d, $J = 5$ Hz, 1H), 9.28 (d, $J = 5$ Hz, 1H), 8.26 (d, $J = 2$ Hz, 2H), 8.09 (d, $J = 8$ Hz, 1H), 7.50–7.14 (m, 19H), 6.96 (d, $J = 8$ Hz, 4H), 2.73 (m, 2H), 1.70 (s, 4H), 1.34 (s, 12H), 1.13 (d, $J = 7$ Hz, 12H), 0.74 (s, 18H) ppm; ^{13}C-NMR (75 MHz, CD_2Cl_2, 300 K) δ [ppm]: 163.6, 156.4, 153.1, 152.7, 147.4, 146.4, 146.3, 144.8, 131.9, 131.6, 131.5, 130.6, 130.4, 130.1, 128.3, 128.2, 127.4, 126.4, 125.3, 125.1, 124.6, 124.4, 124.3, 124.2, 122.7, 121.9, 121.2, 118.9, 118.8, 57.3, 38.4, 32.6, 31.8, 31.6, 29.3, 24.0. IR Spectrum (KBr): $\nu_{\max} = 2958$, 1706, 1660, 1588, 1506, 1414, 1338, 1272, 1200, 1054, 1014, 872, 750, 692, 524 cm^{-1}. UV-Vis (CH_2Cl_2): $\lambda_{\max}$ (ε/M^{-1} cm^{-1}): 590 nm (29 916). FD Mass Spectrum (8 kV): $m/z = 1057.1$ (100%) [M$^+$] (calc. 1057.44). Elemental analysis ($C_{74}H_{76}N_2O_4$): calculated: (%) C 84.05, H 7.24, N 2.65, found: (%) C 84.05, H 7.22, N 2.58.

9-Di(*p*-*tert*-octylphenyl)amino-1,6-diphenoxy-perylene-3,4-dicarboxy anhydride (ID96). A mixture of **3** (500 mg, 0.47 mmol), potassium carbonate (2 g, 50 mmol), KF (40 mg, 0.70 mmol) and *iso*-propanol (500 mL) was stirred and refluxed in a 100 mL mononecked round flask overnight. After cooling down to room temperature, the mixture was poured into water and neutralised by acetic acid. The solution was stirred at 60 °C for 0.5 h. The precipitate was dried and purified by column chromatography using dichloromethane as eluent on silica to give a blue solid (340 mg, 80%).

^{1}H-NMR (300 MHz, CD_2Cl_2, 300 K): $\delta = 9.29$ (m, 2H), 8.16 (s, 2H), 8.10 (d, $J = 8$ Hz, 1H), 7.45–7.11 (m, 16H), 6.95 (d, $J = 8$ Hz, 4H), 1.69 (s, 4H), 1.33 (s, 12H), 0.73 (s, 18H) ppm; ^{13}C-NMR (75 MHz, CD_2Cl_2, 300 K) δ [ppm]: 160.4, 160.4, 157.2, 157.2, 154.6, 154.1, 149.2, 149.2, 147.8, 146.3, 145.0, 131.9, 131.7, 130.6, 130.3, 129.8, 128.3, 128.1, 128.1, 127.5, 126.4, 126.2, 124.7, 124.5, 124.4, 124.3, 122.9, 122.8, 121.0, 120.9, 117.1, 116.2, 115.8, 115.8, 57.3, 56.0, 38.4, 32.6, 31.8, 31.6. IR Spectrum (KBr): ν_{max} = 2952, 1777, 1578, 1504, 1420, 1338, 1270, 1202, 1098, 994, 872, 752, 690 cm^{-1}. UV-Vis (CH_2Cl_2): λ_{max} (ε/M^{-1} cm^{-1}): 606 nm (25 195). FD Mass Spectrum (8 kV): $m/z = 890.3$ (100%) [M$^+$] (calc. 898.17). Elemental analysis ($C_{62}H_{59}NO_5$): calculated: (%) C 82.91, H 6.62, N 1.56, Found: (%) C 82.91, H 6.58, N 1.49.

***N*-(2,6-Di*iso*propylphenyl)-1,6-di(4-trimethylsilanylethynyl-phenoxy)-9-bromo-perylene-3,4-dicarboximide (4).** (2,6-Di*iso*propylphenyl)-1,6,9-tribromoperylene-3,4-dicarboximide (1 g, 1.4 mmol), 4-trimethylsilanylethynyl-phenol (0.80 g, 2.8 mmol) and potassium carbonate (0.40 g, 2.8 mmol) were stirred in NMP (150 mL) at 80 °C for 5 h. After cooling down to room temperature, the reaction mixture was poured into a mixture of water and hydrochloric acid (4 : 1). The resulting precipitate was washed with water and dried. The desired product was purified by column chromatography on silica gel using dichloromethane and pentane (1 : 2) as eluent to give a red solid (0.9 g, 58%).

^{1}H-NMR (300 MHz, CD_2Cl_2, 300 K): $\delta = 9.27$ (d, $J = 8$ Hz, 1H), 9.04 (d, $J = 8$ Hz, 1H), 8.31 (m, 3H), 7.88 (d, $J = 8$ Hz, 1H), 7.67 (t, 1H), 7.50 (m, 5H), 7.34 (d, $J = 8$ Hz, 2H), 7.09 (m, 4H), 2.72 (m, 2H), 1.13 (m, 54H) ppm; ^{13}C-NMR (75 MHz, CD_2Cl_2, 300 K) δ [ppm]: 163.4, 163.3, 156.2, 156.1, 153.0, 152.9, 146.3, 134.4, 132.2, 131.8, 131.4, 131.3, 130.9, 129.9, 129.8, 129.2, 128.2, 127.9, 127.7, 127.4, 126.0, 125.8, 125.7, 124.4, 124.3, 122.6, 122.5, 120.0, 119.8, 119.7, 118.5, 106.5, 106.4, 91.0, 29.4, 24.1, 18.7, 11.6. IR Spectrum (KBr): ν_{max} = 2941, 2864, 2154, 1709, 1670, 1593, 1496, 1412, 1333, 1269, 1201, 1068, 1012, 995, 877, 831, 789 cm^{-1}. UV-Vis (CH_2CL_2): λ_{max} (ε/M^{-1} cm^{-1}): 513 (47541). FD Mass Spectrum (8 kV): $m/z = 1038.2$ (100%) [M$^+$] (calc. 1105.43). Elemental analysis ($C_{68}H_{74}BrNO_4Si_2$): calculated: (%) C 83.28, H 7.67, N 1.35, found: (%) C 83.41, H 7.63, N 1.41.

***N*-(2,6-Di*iso*propylphenyl)-1,6-di(4-ethynylphenoxy)-9-bromo-perylene-3,4-dicarboximide (5).** Compound **4** (500 mg, 0.45 mmol) was dissolved in THF (50 mL) in a 100 mL Schlenk flask under argon. A THF solution of tetra-*n*-butylammonium fluoride (0.56 g, 1.78 mmol) was injected and the reaction mixture was stirred for 30 min at room temperature. The solution was diluted with dichloromethane (200 mL), and then extracted with aqueous hydrochloric acid (100 mL, 6 M). The organic phase was separated, washed with distilled water (100 mL) and dried over magnesium sulfate. The solvents were removed under reduced pressure, and the crude product was purified by column chromatography on silica gel with dichloromethane to give a red solid **5** (250 mg, 70%).

^{1}H-NMR (300 MHz, CD_2Cl_2, 300 K): $\delta = 9.29$ (d, $J = 9$ Hz, 1H), 9.06 (d, $J = 9$ Hz, 1H), 8.37 (d, $J = 9$ Hz, 1H), 8.32 (s, 1H), 8.30(s, 1H), 7.90 (d, $J = 9$ Hz, 1H), 7.70 (t, 1H), 7.50 (m, 5H), 7.34 (d, $J = 8$ Hz, 2H), 7.10 (m, 4H), 3.11 (s, 2H), 2.71 (m, 2H), 1.13 (d, $J = 7$ Hz, 12H) ppm; ^{13}C-NMR (75 MHz, CD_2Cl_2, 300 K) δ [ppm]: 163.3, 156.6, 156.5, 152.8, 152.7, 146.3, 134.5, 132.3, 131.8, 131.2, 130.9, 129.3, 129.2, 128.5, 128.0, 127.9, 127.8, 127.3, 126.1, 125.5, 124.4, 124.4, 122.6, 122.5, 118.5, 118.2, 118.1, 82.9, 77.4, 29.4, 24.0, 21.4. IR Spectrum (KBr): ν_{max} = 3259, 2960, 2873, 2349, 1701, 1664, 1593, 1496, 1333, 1265, 1205, 1057, 872, 829, 804, 741 cm^{-1}. UV-Vis (CH_2Cl_2): λ_{max} (ε/M^{-1} cm^{-1}): 509 nm (19 625). FD Mass Spectrum (8 kV): $m/z = 791.8$ (100%) [M$^+$] (calc. 792.74). Elemental analysis ($C_{50}H_{34}BrNO_4$) calculated: (%) C 75.76, H 4.32, N 1.77, found: C 76.02, H 4.37, N 1.59.

***N*-(2,6-Di*iso*propylphenyl)-1,6-di((2,3,4,5-tetraphenyl)phenyl-phenoxy)-9-bromo-perylene-3,4-dicarboximide (6).** A mixture of **5** (200 mg, 0.25 mmol), tetraphenylcyclopentadienone (245 mg, 0.63 mmol) and *m*-xylene (15 ml) was refluxed overnight. The solvents were removed under reduced pressure, and the crude product was purified by column chromatography on silica gel with toluene to give a red solid (270 mg, 75%).

^{1}H-NMR Spectrum (300 MHz, CD_2Cl_2, 300 K) δ[ppm]: 9.32 (d, $J = 9$ Hz, 1H), 9.09 (d, $J = 9$ Hz, 1H), 8.37 (d, $J = 9$ Hz, 1H), 8.22 (s, 1H), 8.22 (s, 1H), 7.90 (d, $J = 9$ Hz, 1H), 7.70 (t, 1H), 7.56 (s, 2H), 7.50 (m, 1H), 7.36 (d, $J = 8$ Hz, 2H), 7.24–7.25 (m, 14H), 7.00–6.80 (m, 34H), 2.72 (m, 2H), 1.15 (d, $J = 7$ Hz, 12H); ^{13}C-NMR (75 MHz, CD_2Cl_2, 300 K) δ [ppm]: 163.6, 154.8, 153.2, 152.7, 147.3, 146.4, 146.3, 144.8, 142.1, 142.0, 141.2, 140.8, 140.4, 140.3, 140.1, 139.8, 139.7, 138.1, 138.0, 132.1, 131.9, 131.9, 131.8, 131.6, 131.5, 131.4, 130.4, 130.2, 129.3, 128.5, 128.1, 128.0, 127.9, 127.4, 127.3, 127.1, 126.9, 126.6, 126.0, 125.6, 124.5, 124.3, 124.0, 122.7, 121.8, 121.1, 118.2, 118.1, 57.3, 38.4, 32.6, 31.8, 31.6, 29.4, 24.1, 21.5. IR Spectrum (KBr): ν_{max} = 3026, 2925, 2868, 2335, 1709, 1670, 1597, 1496, 1441, 1333, 1271, 1201, 1072, 1030, 970, 841, 762 cm^{-1}. UV-Vis (CH_2Cl_2): λ_{max} (ε/M^{-1} cm^{-1}): 513 nm (32 584). FD Mass Spectrum (8 kV): $m/z = 1505.4$ (100%) [M$^+$] (Calc. 1505.68). Elemental Analysis ($C_{106}H_{74}BrNO_4$) Calculated: (%) C 84.56, H 4.95, N 5.31, found: C 84.04, H 5.49, N 0.87, S 7.31.

***N*-(2,6-Di*iso*propylphenyl)-9-di(*p*-*tert*-octylphenyl)amino-1,6-di((2,3,4,5-tetraphenyl)phenyl-phenoxy)-perylene-3,4-dicarboximide (7).** A mixture of **6** (150 mg, 0.10 mmol), *p*,*p*′-di-*tert*-octyldiphenylamine (60 mg, 0.15 mmol), tris-(dibenzylideneacetone)-dipalladium(0) (20 mg, 0.02 mmol), tri-*tert*-butylphosphine (20 mg, 0.10 mmol), sodium-*tert*-butoxide (20 mg, 0.15 mmol) and dry toluene (100 mL) was stirred at 80 °C in an argon atmosphere for one day. The solvent was removed under evaporation. The crude product was purified by column chromatography using dichloromethane and pentane (1 : 2) as eluent on silica to give a blue solid (150 g, 82%).

^{1}H-NMR Spectrum (300 MHz, CD_2Cl_2, 300 K) δ[ppm]: 9.20 (m, 2H), 8.20 (s, 2H), 8.10 (d, $J = 8$ Hz, 1H), 7.57 (d, $J = 2$ Hz, 2H), 7.50 (m, 1H), 7.38–7.15 (m, 22H), 6.97–6.82 (m, 38H), 2.73 (m, 2H), 1.71 (s, 4H), 1.36 (s, 12H), 1.15 (d, $J = 7$ Hz, 12H), 0.76 (s, 18H); ^{13}C-NMR (62.5 MHz, CD_2Cl_2, 300 K) δ [ppm]: 163.6, 154.8, 153.2, 152.7, 147.3, 146.4, 146.3, 144.8, 142.1, 142.0, 141.2, 140.8, 140.4, 140.3, 140.1, 139.8, 139.7, 138.1, 138.0, 132.1, 131.9, 131.9, 131.8, 131.6, 131.5, 131.4, 130.4, 130.2, 129.3, 128.5, 128.1, 128.0, 127.9, 127.4, 127.3, 127.1, 126.9, 126.6, 126.0, 125.6, 124.5, 124.3, 124.0, 122.7, 121.8, 121.1, 118.2, 118.1, 57.3, 38.4, 32.6, 31.8, 31.6, 29.4, 24.1, 21.5. IR Spectrum (KBr): ν_{max} = 2956, 2868, 1706, 1662, 1600, 1504, 1442, 1332, 1272, 1204, 1072, 1016, 878, 828, 762, 698 cm^{-1}. UV-Vis (CH_2Cl_2): λ_{max} (ε/M^{-1} cm^{-1}):

590 nm (31 646). FD Mass Spectrum (8 kV): m/z = 1819.7 (100%) [M^+] (Calc. 1818.43). Elemental analysis ($C_{134}H_{116}N_2O_4$): calculated: (%) C 88.51, H 6.43, N 1.54, found: (%) C 87.94, H 6.42, N 1.52.

9-Di(*p-tert*-octylphenyl)amino-1,6-di((2,3,4,5-tetraphenyl)phenylphenoxy)-perylene-3,4-dicarboxy anhydride (ID115). A mixture of **7** (100 mg, 0.05 mmol), potassium carbonate (100 mg, 1.8 mmol) and *iso*-propanol (20 mL) was stirred and refluxed in a 100 mL mono-necked round flask overnight. After the reaction mixture was cooled to 40 °C, 20 mL of acetic acid solution (50%) was added to the reaction mixture. The solution was stirred at 60 °C for 2 h. The precipitate was dried and purified by column chromatography using dichloromethane as eluent on silica to give a blue solid (50 mg, 60%).

^{1}H-NMR Spectrum (300 MHz, CD_2Cl_2, 300 K) δ[ppm]: 9.20 (m, 2H), 8.11 (s, 1H), 8.07 (s, 2H), 7.58 (d, J = 2 Hz, 2H), 7.36–7.18 (m, 20H), 7.00–6.83 (m, 39H), 1.71 (s, 4H), 1.34 (s, 12H), 0.75 (s, 18H); ^{13}C-NMR (75 MHz, CD_2Cl_2, 300 K) δ [ppm]: 160.3, 160.2, 154.4, 153.5, 153.0, 148.0, 146.3, 145.0, 142.1, 142.0, 141.2, 140.8, 140.4, 140.3, 140.1, 139.8, 139.7, 138.7, 138.5, 132.2, 131.9, 131.8, 131.8, 131.7, 131.4, 130.2, 130.1, 128.9, 128.8, 127.9, 127.8, 127.5, 127.4, 127.2, 126.9, 126.6, 126.1, 125.9, 125.7, 125.3, 124.0, 122.9, 118.7, 118.5, 117.1, 116.2, 57.3, 38.4, 32.6, 31.8. IR Spectrum (KBr): ν_{max} = 2952, 1774, 1600, 1504, 1442, 1336, 1272, 1208, 1098, 994, 938, 830, 762, 698 cm^{-1}. UV-Vis (CH_2Cl_2): λ_{max} (ε/M^{-1} cm^{-1}): 606 nm (18 774). FD Mass Spectrum (8 kV): m/z = 1506.5 (100%) [M^+] (calc. 1506.96). Elemental analysis ($C_{122}H_{99}NO_5$): calculated: (%) C 88.32, H 6.01, N 0.84, found: (%) C 87.77, H 6.16, N 0.78.

Acknowledgements

We acknowledge the financial support by the Deutsche Forschungsgemeinschaft (DFG) priority program (SPP 1355) Elementary Processes of Organic Photovoltaics.

References

1 U. Bach, D. Lupo, P. Comte, J. E. Moser, F. Weissortel, J. Salbeck, H. Spreitzer and M. Grätzel, *Nature*, 1998, **395**, 583–585.
2 B. O'Regan and M. Grätzel, *Nature*, 1991, **353**, 737–740.
3 S. A. Haque, E. Palomares, B. M. Cho, A. N. M. Green, N. Hirata, D. R. Klug and J. R. Durrant, *J. Am. Chem. Soc.*, 2005, **127**, 3456–3462.
4 B. C. O'Regan and J. R. Durrant, *J. Phys. Chem. B*, 2006, **110**, 8544–8547.
5 S. Y. Huang, G. Schlichthorl, A. J. Nozik, M. Grätzel and A. J. Frank, *J. Phys. Chem. B*, 1997, **101**, 2576–2582.
6 B. A. Gregg, F. Pichot, S. Ferrere and C. L. Fields, *J. Phys. Chem. B*, 2001, **105**, 1422–1429.
7 K. Tennakone, V. P. S. Perera, I. R. M. Kottegoda, L. A. A. De Silva, G. Kumara and A. Konno, *J. Electron. Mater.*, 2001, **30**, 992–996.
8 G. Kumara, K. Tennakone, V. P. S. Perera, A. Konno, S. Kaneko and M. Okuya, *J. Phys. D: Appl. Phys.*, 2001, **34**, 868–873.
9 E. Palomares, J. N. Clifford, S. A. Haque, T. Lutz and J. R. Durrant, *J. Am. Chem. Soc.*, 2003, **125**, 475–482.
10 A. Zaban, S. G. Chen, S. Chappel and B. A. Gregg, *Chem. Commun.*, 2000, 2231–2232.
11 Z. Zhang, S. M. Zakeeruddin, B. C. O'Regan, R. Humphry-Baker and M. Grätzel, *J. Phys. Chem. B*, 2005, **109**, 21818–21824.
12 Z. Zhang, N. Evans, S. M. Zakeeruddin, R. Humphry-Baker and M. Grätzel, *J. Phys. Chem. C*, 2007, **111**, 398–403.
13 J. E. Kroeze, N. Hirata, S. Koops, M. K. Nazeeruddin, L. Schmidt-Mende, M. Grätzel and J. R. Durrant, *J. Am. Chem. Soc.*, 2006, **128**, 16376–16383.
14 H. Choi, C. Baik, S. O. Kang, J. Ko, M.-S. Kang, M. K. Nazeeruddin and M. Grätzel, *Angew. Chem., Int. Ed.*, 2008, **47**, 327–330.
15 A. Burke, L. Schmidt-Mende, S. Ito and M. Grätzel, *Chem. Commun.*, 2007, 234–236.
16 R. Chen, X. Yang, H. Tian, X. Wang, A. Hagfeldt and L. Sun, *Chem. Mater.*, 2007, **19**, 4007–4015.
17 H. Choi, J. K. Lee, K. Song, S. O. Kang and J. Ko, *Tetrahedron*, 2007, **63**, 3115–3121.
18 D. P. Hagberg, T. Edvinsson, T. Marinado, G. Boschloo, A. Hagfeldt and L. Sun, *Chem. Commun.*, 2006, 2245–2247.
19 K. Hara, T. Horiguchi, T. Kinoshita, K. Sayama, H. Sugihara and H. Arakawa, *Chem. Lett.*, 2000, 316–317.
20 K. Hara, T. Sato, R. Katoh, A. Furube, Y. Ohga, A. Shinpo, S. Suga, K. Sayama, H. Sugihara and H. Arakawa, *J. Phys. Chem. B*, 2003, **107**, 597–606.
21 T. Horiuchi, H. Miura, K. Sumioka and S. Uchida, *J. Am. Chem. Soc.*, 2004, **126**, 12218–12219.
22 S. Ito, S. M. Zakeeruddin, R. Humphry-Baker, P. Liska, R. Charvet, P. Comte, M. K. Nazeeruddin, P. Pechy, M. Takata, H. Miura, S. Uchida and M. Grätzel, *Adv. Mater.*, 2006, **18**, 1202–1205.
23 S. Kim, J. K. Lee, S. O. Kang, J. Ko, J. H. Yum, S. Fantacci, F. De Angelis, D. Di Censo, M. K. Nazeeruddin and M. Grätzel, *J. Am. Chem. Soc.*, 2006, **128**, 16701–16707.
24 T. Kitamura, M. Ikeda, K. Shigaki, T. Inoue, N. A. Anderson, X. Ai, T. Lian and S. Yanagida, *Chem. Mater.*, 2004, **16**, 1806–1812.
25 A. Konno, G. R. A. Kumara, S. Kaneko, B. Onwona-Agyeman and K. Tennakone, *Chem. Lett.*, 2007, **36**, 716–717.
26 Y. Kurashige, T. Nakajima, S. Kurashige, K. Hirao and Y. Nishikitani, *J. Phys. Chem. A*, 2007, **111**, 5544–5548.
27 M. Liang, W. Xu, F. Cai, P. Chen, B. Peng, J. Chen and Z. Li, *J. Phys. Chem. C*, 2007, **111**, 4465–4472.
28 F. S. Meng, Q. H. Yao, J. G. Shen, F. L. Li, C. H. Huang, K. C. Chen and H. Tian, *Synth. Met.*, 2003, **137**, 1543–1544.
29 R. Mosurkal, L. Hoke, S. A. Fossey, L. A. Samuelson, J. Kumar, D. Waller and R. A. Gaudiana, *J. Macromol. Sci., Part A: Pure Appl. Chem.*, 2006, **43**, 1907–1922.
30 K. Sayama, M. Sugino, H. Sugihara, Y. Abe and H. Arakawa, *Chem. Lett.*, 1998, 753–754.
31 K. Sayama, S. Tsukagoshi, K. Hara, Y. Ohga, A. Shinpou, Y. Abe, S. Suga and H. Arakawa, *J. Phys. Chem. B*, 2002, **106**, 1363–1371.
32 K. Takahashi, T. Nakanishi, T. Yamaguchi, J.-i. Nakamura and K. Murata, *Chem. Lett.*, 2005, **34**, 714–715.
33 S. Tan, J. Zhai, H. Fang, T. Jiu, J. Ge, Y. Li, L. Jiang and D. Zhu, *Chem.–Eur. J.*, 2005, **11**, 6272–6276.
34 K. R. J. Thomas, J. T. Lin, Y.-C. Hsu and K.-C. Ho, *Chem. Commun.*, 2005, 4098–4100.
35 Z.-S. Wang, Y. Cui, K. Hara, Y. Dan-oh, C. Kasada and A. Shinpo, *Adv. Mater.*, 2007, **19**, 1138–1141.
36 Z.-S. Wang, F.-Y. Li and C.-H. Huang, *J. Phys. Chem. B*, 2001, **105**, 9210–9217.
37 C. Li, J. Schöneboom, Z. Liu, N. G. Pschirer, P. Erk, A. Herrmann and K. Müllen, *Chem.–Eur. J.*, 2009, **15**, 878–884.
38 Z. Liu, C. Li, M. Wagner, Y. Avlasevich, A. Herrmann and K. Müllen, *Chem. Commun.*, 2008, 5028–5030.
39 J. Hofkens, M. Maus, T. Gensch, T. Vosch, M. Cotlet, F. Köhn, A. Herrmann, K. Müllen and F. De Schryver, *J. Am. Chem. Soc.*, 2000, **122**, 9278–9288.
40 A. J. Breeze, A. Salomon, D. S. Ginley, B. A. Gregg, H. Tillmann and H. H. Horhold, *Appl. Phys. Lett.*, 2002, **81**, 3085–3087.
41 J. Cremer and P. Bäuerle, *J. Mater. Chem.*, 2006, **16**, 874–884.
42 G. M. Hasselman, D. F. Watson, J. R. Stromberg, D. F. Bocian, D. Holten, J. S. Lindsey and G. J. Meyer, *J. Phys. Chem. B*, 2006, **110**, 25430–25440.
43 D. A. Heggie, B. L. MacDonald and I. G. Hill, *J. Appl. Phys.*, 2006, **100**, 104505.
44 G. Horowitz, F. Kouki, P. Spearman, D. Fichou, C. Nogues, X. Pan and F. Garnier, *Adv. Mater.*, 1996, **8**, 242–245.
45 J. Hua, F. Meng, J. Li, F. Ding, X. Fan and H. Tian, *Eur. Polym. J.*, 2006, **42**, 2686–2694.
46 J. Jacob, S. Sax, T. Piok, E. J. W. List, A. C. Grimsdale and K. Müllen, *J. Am. Chem. Soc.*, 2004, **126**, 6987–6995.

47 B. A. Jones, M. J. Ahrens, M.-H. Yoon, A. Facchetti, T. J. Marks and M. R. Wasielewski, *Angew. Chem., Int. Ed.*, 2004, **43**, 6363–6366.
48 V. Lemaur, M. Steel, D. Beljonne, J.-L. Bredas and J. Cornil, *J. Am. Chem. Soc.*, 2005, **127**, 6077–6086.
49 J. Li, F. Dierschke, J. Wu, A. C. Grimsdale and K. Müllen, *J. Mater. Chem.*, 2006, **16**, 96–100.
50 E. E. Neuteboom, S. C. J. Meskers, P. A. Van Hal, J. K. J. Van Duren, E. W. Meijer, R. A. J. Janssen, H. Dupin, G. Pourtois, J. Cornil, R. Lazzaroni, J.-L. Bredas and D. Beljonne, *J. Am. Chem. Soc.*, 2003, **125**, 8625–8638.
51 L. Schmidt-Mende, A. Fechtenkotter, K. Müllen, E. Moons, R. H. Friend and J. D. MacKenzie, *Science*, 2001, **293**, 1119–1122.
52 W. S. Shin, H.-H. Jeong, M.-K. Kim, S.-H. Jin, M.-R. Kim, J.-K. Lee, J. W. Lee and Y.-S. Gal, *J. Mater. Chem.*, 2006, **16**, 384–390.
53 M. Sommer, S. M. Lindner and M. Thelakkat, *Adv. Funct. Mater.*, 2007, **17**, 1493–1500.
54 L. Tan, M. D. Curtis and A. H. Francis, *Chem. Mater.*, 2004, **16**, 2134–2141.
55 F. Würthner, Z. Chen, F. J. M. Hoeben, P. Osswald, C.-C. You, P. Jonkheijm, J. von Herrikhuyzen, A. P. H. J. Schenning, P. P. A. M. van der Schoot, E. W. Meijer, E. H. A. Beckers, S. C. J. Meskers and R. A. J. Janssen, *J. Am. Chem. Soc.*, 2004, **126**, 10611–10618.
56 X. Zhan, Z. a. Tan, B. Domercq, Z. An, X. Zhang, S. Barlow, Y. Li, D. Zhu, B. Kippelen and S. R. Marder, *J. Am. Chem. Soc.*, 2007, **129**, 7246–7247.
57 C. Li, J. H. Yum, S. J. Moon, A. Herrmann, F. Eickemeyer, N. G. Pschirer, P. Erk, J. Schöneboom, K. Müllen, M. Grätzel and M. K. Nazeeruddin, *ChemSusChem*, 2008, **1**, 615–618.
58 T. Edvinsson, C. Li, N. Pschirer, J. Schoeneboom, F. Eickemeyer, R. Sens, G. Boschloo, A. Herrmann, K. Müllen and A. Hagfeldt, *J. Phys. Chem. C*, 2007, **111**, 15137–15140.
59 Y. Geerts, H. Quante, H. Platz, R. Mahrt, M. Hopmeier, A. Bohm and K. Müllen, *J. Mater. Chem.*, 1998, **8**, 2357–2369.
60 H. Quante and K. Müllen, *Angew. Chem., Int. Ed. Engl.*, 1995, **34**, 1323–1325.
61 U. Rohr, C. Kohl, K. Müllen, A. van de Craats and J. Warman, *J. Mater. Chem.*, 2001, **11**, 1789–1799.
62 J. Qu, D. Liu, S. De Feyter, J. Zhang, F. C. De Schryver and K. Müllen, *J. Org. Chem.*, 2003, **68**, 9802–9808.
63 J. Qu, N. G. Pschirer, D. Liu, A. Stefan, F. C. De Schryver and K. Müllen, *Chem.–Eur. J.*, 2004, **10**, 528–537.
64 S. Ferrere and B. A. Gregg, *New J. Chem.*, 2002, **26**, 1155–1160.
65 S. Brunauer, P. H. Emmett and E. Teller, *J. Am. Chem. Soc.*, 1938, **60**, 309–319.
66 N. Koumura, Z.-S. Wang, S. Mori, M. Miyashita, E. Suzuki and K. Hara, *J. Am. Chem. Soc.*, 2006, **128**, 14256–14257.
67 R. Ahlrichs, M. Bär, M. Häser, H. Horn and C. Kölmel, *Chem. Phys. Lett.*, 1989, **162**, 165–169.
68 A. D. Becke, *Phys. Rev. A: At., Mol., Opt. Phys.*, 1988, **38**, 3098–3100.
69 K. Eichkorn, F. Weigend, O. Treutler and R. Ahlrichs, *Theor. Chem. Acc.*, 1997, **97**, 119–124.
70 R. Bauernschmitt and R. Ahlrichs, *Chem. Phys. Lett.*, 1996, **256**, 454–464.
71 R. Bauernschmitt and R. Ahlrichs, *J. Chem. Phys.*, 1996, **104**, 9047–9052.
72 A. D. Becke, *J. Chem. Phys.*, 1993, **98**, 5648–5652.
73 A. Schäfer, H. Horn and R. Ahlrichs, *J. Chem. Phys.*, 1992, **97**, 2571–2577.